Journal of Remote Sensing
A SCIENCE PARTNER JOURNAL

REVIEW ARTICLE

Urban Core Greening Balances Browning in Urban Expansion Areas in China during Recent Decades

Xiaoxin Zhang[1*], Martin Brandt[1], Xiaoye Tong[1], Xiaowei Tong[2], Wenmin Zhang[1], and Rasmus Fensholt[1]

[1]Department of Geosciences and Natural Resource Management, University of Copenhagen, Copenhagen, Denmark. [2]Key Laboratory for Agro-ecological Processes in Subtropical Region, Institute of Subtropical Agriculture, Chinese Academy of Sciences, Changsha, China.

*Address correspondence to: xzh@ign.ku.dk

Citation: Zhang X, Brandt M, Tong X, Tong X, Zhang W, Fensholt R. Urban Core Greening Balances Browning in Urban Expansion Areas in China during Recent Decades. *J. Remote Sens.* 2024;4:Article 0112. https://doi.org/10.34133/remotesensing.0112

Submitted 3 July 2022
Accepted 10 January 2024
Published 8 February 2024

China has experienced a rapid urbanization during recent decades, strongly affecting vegetation dynamics in areas undergoing a transformation from rural to urban areas. At the same time, national greening policies have been implemented to promote urban sustainability and urban greening in China in recent years. However, it is unclear how urban greening compensates vegetation losses from urban expansion at national scale. Here, we use Moderate Resolution Imaging Spectroradiometer and Landsat satellite normalized difference vegetation index time series to study 974 major cities (urban area > 20 km^2) in China during 2000 to 2020 and develop an urban vegetation change typology including 5 types of vegetation dynamics (greening, browning, stable, reversal, and recovery). We document a rapid urban expansion associated with a browning in urban areas before 2011, followed by widespread regreening of the urban areas after 2011. This recovery in greenness was found in 63.45% of the cities, while 14.68% showed a continuous browning, and 8.13% a continuous greening. Our findings reveal to what extent, where, and when vegetation browning from urban expansion is balanced by urban greening in urban core areas, which may indicate that initial vegetation losses are offset by urban greening initiatives.

Introduction

More than two-thirds of the human population is projected to reside in urban areas by 2030 [1]. This requires an expansion of urban areas with considerable losses in vegetation cover caused by the conversion of natural and agricultural land into impervious surfaces [2,3]. However, urban land does not necessarily exclude vegetation, and urban greening is a well-known global phenomenon [2,4]. Vegetation in urban areas is typically planted and managed and provides several ecosystem services ranging from the mitigation of air pollution [5], traffic noise [6], the reduction of air temperature [7], to the improvement of people's physical and mental health [8,9]. The ecological services available from urban vegetation naturally depend on the implementation year of a given urban greening initiative. Consequently, since urban areas and associated green infrastructure do not grow homogeneously, there is often a heterogeneous and nonlinear pattern of vegetation dynamic across and within urban areas [10].

Previous studies have documented change of urban vegetation using satellite data [11–13]; however, in many studies, an assumption is made that vegetation changes are linear over time and distributed homogeneously within city areas, which may not always reflect reality [8,9]. Indeed, there are large spatial differences and even diverging vegetation trends within cities [14], and varying policies and management can lead to nonlinear temporal changes. Only a few studies have recently studied nonlinear urban vegetation changes using satellite time series, revealing different types and periods of changes for single cities [10,14]. Interestingly, Zhang et al. [15] found that aboveground biomass in urban areas in China increased over the recent decades, which compensates for initial aboveground biomass caused by the expansion of urban areas in earlier years, a phenomenon referred to as "green recovery".

If using linear trend analysis, most large cities in China show an overall negative trend in vegetation cover during 2000 to 2018, reflecting the conversion of green landscapes to built-up areas [13]. However, this approach is likely not to capture adequately the attempt from the Chinese government to improve the urban environment. This has been done by implementing a series of regulations and policies, such as the "Urban Greening Policies" starting 1992, which includes tree plantations in public and residential areas [16,17]. These projects are observed as green recovery in satellite time series [2,14]. One of the current strategies in China is named "Ecological Civilization" and aims at balancing economic development and environmental protection [18,19]. To evaluate the effect of such programs, detecting and quantifying nonlinear vegetation dynamics in urban areas is essential. Previous studies often either select example cities [14] or merge all urban areas at national scale [15] and also do not consider heterogeneity of trends within individual cities.

Here, we use normalized difference vegetation index (NDVI) time series to study nonlinear vegetation changes for all major cities (urban areas >20 km^2) in China during 2000 to 2020. We classify changes in NDVI into 5 change types: greening, browning, recovery (change from browning to greening), reversal (greening to browning), and stable. Trends and change types are studied at city level using coarse and robust Moderate Resolution Imaging Spectroradiometer (MODIS) time series and additionally with moderate-resolution Landsat time series revealing heterogeneous patterns within cities.

Datasets

Satellite image time series for urban vegetation monitoring

MODIS vegetation index time series

We used time series combining the MODIS Collection 6 Vegetation Index (VI) product from MOD13Q1 C6 (Terra, https://lpdaac.usgs.gov/products/mod13q1v006/) and MYD13Q1 C6 (Aqua, https://lpdaac.usgs.gov/products/myd13q1v061/) to study dynamics in vegetation greenness for the period 2001 to 2020. Both MODIS products are provided as 16-d image composites at a spatial resolution of 250 m and are computed from atmospherically corrected bidirectional near-daily surface reflectance masked for water, clouds, heavy aerosols, and cloud shadows. Compared to vegetation indexes such as enhanced vegetation index, NDVI values is more responsive to changes in sparse vegetation cover, thereby producing a wider range in data values (Fig. S1). This makes NDVI a good choice for monitoring vegetation dynamics in sparsely vegetated regions, such as urban areas [13,20,21]. We filtered observation flagged as snow, water, and cloud cover using the embedded quality data (SummaryQA ≤ 1) available in Google Earth Engine. Pixels with less than 10 good-quality observations per year (8.21%) were masked (Fig. 1A and B). Maximum monthly NDVI was calculated, and no-data pixels were filled with mean values from a 4-months moving window (previous 2 mo and following 2 mo). Annual averages values were then calculated from the monthly NDVI time series for the period 2001 to 2020. The relatively coarse spatial resolution does not reveal details, but the time series based on MODIS 8-d composite observations provides robust and reliable results at the level of individual cities.

Landsat time series

Landsat time series were used to study changes in vegetation greenness with a higher level of spatial details within urban areas at a 30-m × 30-m resolution. We used the Landsat Surface Reflectance Climate Data Record which includes Landsat 5, 7 and 8, all corrected for atmospheric interference and geometric distortions [22] (Fig. 1C and D). We masked pixels flagged as cloudy, cloud shadow, snow, and water and used annual medoid composites of NDVI [23]. A total of 4.69% of the pixels in the urban areas have less than 10 good-quality observations per year and were not used for further analyses (Fig. 1C and E).

Ancillary datasets for the definition of urban boundaries

GlobeLand30 land cover dataset

GlobeLand30 (GL30) land cover maps are produced by the National Geomatics of China at 30-m spatial resolution using Landsat satellite images every 5 years during 2000 to 2020, with an overall accuracy of 85.5% [24,25]. Land cover is mapped for 10 classes including water, wetland, artificial surfaces, cultivated land, forest, shrub land, grassland, bare land, tundra, and permanent snow/ice [24]. We used the class of artificial surfaces to define the urban areas in 2020 and 2000.

Nighttime light data

Urban areas from the GL30 classification are not always spatially adjoined and can form isolated clusters of built-up areas belonging to the same city (Fig. S2). To merge several clustered belonging to the same city, we used the Suomi National Polar-orbiting Partnership (NPP) Satellite Visible Infrared Imaging Radiometer Suite (VIIRS) nighttime light data at a spatial resolution of 500 m, which have been widely used to estimate human activities and to extract urban areas [26]. We calculated the yearly mean nighttime lights using cloud-free pixels (cloud-free coverages = 0) from monthly NPP-VIIRS data for 2020 [27].

Methodology

To study urban vegetation trends and to detect the change types, we developed a framework consisting of 3 main steps: (a) the definition of urban boundaries; (b) the estimation of monotonic trends in urban greenness; and (c) the segmentation of change types related to urban vegetation at the level of individual cities using MODIS NDVI time series and within urban areas at the pixel level using Landsat time series. A flowchart summarizing the workflow is provided in Fig. S3.

Definition of urban boundaries

First, the GL30 land cover map was used to extract information about built-up areas using the class of artificial surfaces for both 2000 and 2020. We then filled nonurban pixels within the urban boundaries, which are typically urban green spaces or lakes. To limit the effect of changes in greenness to built-up areas, we masked all water surfaces and croplands located within urban areas based on the land cover map from 2000. We then aggregated built-up areas to 250 m to match the resolution of the MODIS NDVI dataset.

Next, we used the average monthly nighttime lights data for 2020 to merge built-up clusters into urban megaregions (500-m spatial resolution) with an empirical threshold (DN ≥ 12) [28] (Fig. S2). Erroneously merged cities were separated using district-level administrative boundary information provided by the National Geomatics Center of China [29]. In these urban areas, built-up areas larger than 20 km^2 in 2020 are here considered as major urban areas or cities, resulting in 974 cities in total. Built-up areas being present both in 2000 and 2020 are considered as urban core, while urban areas not present in 2000 but in 2020 were defined as urban expansion areas.

Urban vegetation change monitoring

As a benchmark analysis, we averaged MODIS NDVI for each year from 2001 to 2020 and over all cities (974) to understand the change in urban greenness at national scale. Then, to understand the diversity of trends observed between cities, a linear regression was used to study monotonic greenness trends over 2001 to 2020 using annually averaged MODIS NDVI for each city.

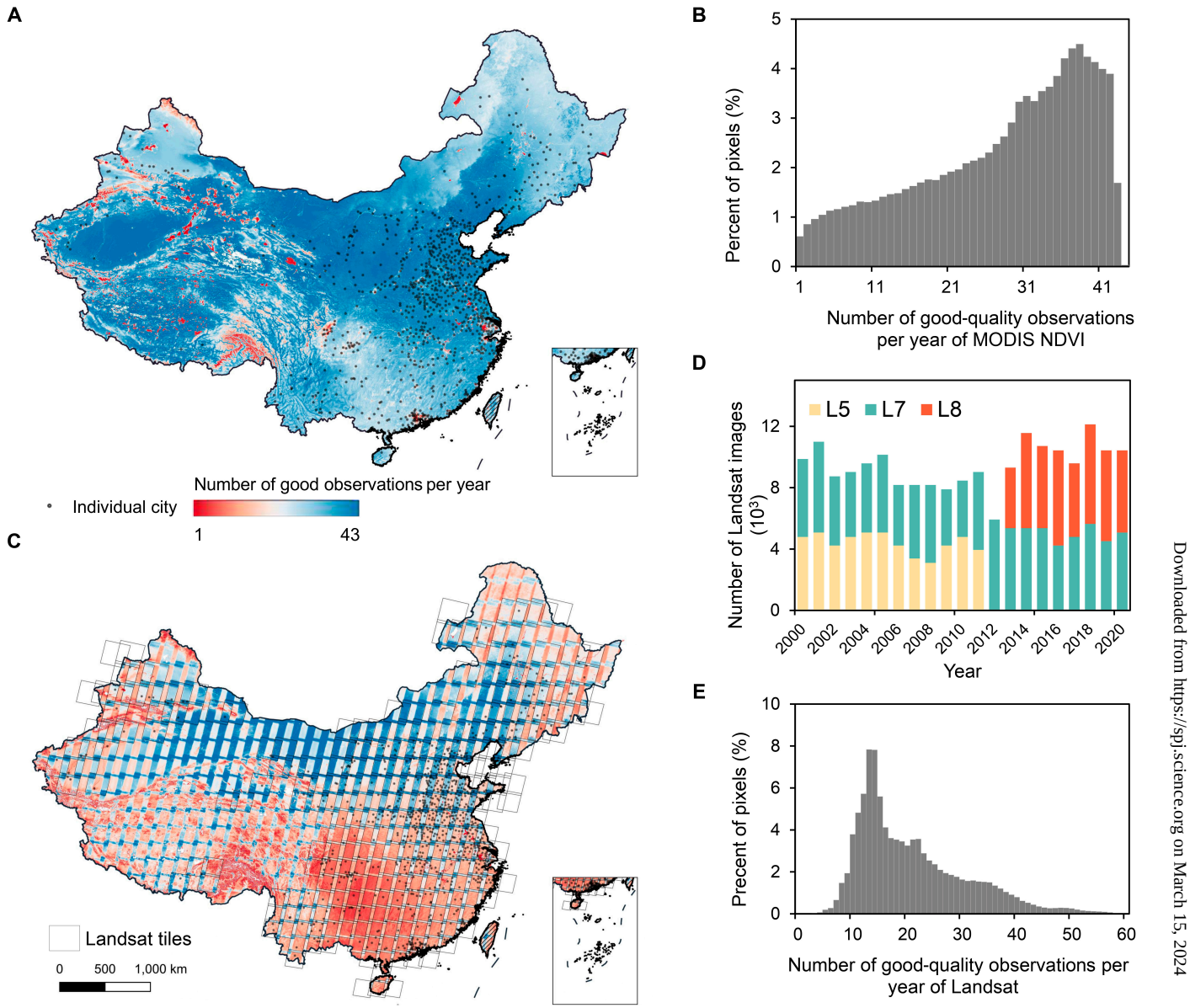

Fig. 1. Availability of MODIS and Landsat images. (A) The spatial distribution of the mean number of annual good-quality observations (SummaryQA ≤ 1) for each 250-m × 250-m pixel in China during 2001 to 2020. (B) Histogram of averaged number of observations of available good-quality MODIS pixels (n =1,629,836) for the study area. (C) Spatial distribution of the average number of good-quality observations for each Landsat pixel (30 m × 30 m) in China during 2000 to 2020. (D) The number of images by sensors Landsat 5/7/8 (L5/L7/L8) per single year. (E) Histogram of averaged good-quality observations of Landsat pixels (n = 130,940,116) for the study area.

Change types of urban vegetation greenness

The transformation of urban land uses is multidirectional, which can change between urban and other land cover/use types, for example agriculture, shrubland, or forest [10]. In this study, we focus on vegetation greenness changes within urban cores (both urban in 2000 and 2020) and newly urbanized areas (not urban in 2000 but in 2020). Using a time series segmentation approach (see detailed method below) focusing on abrupt changes, we classified mainly 5 change types of NDVI time series as described in the following sections (Fig. 2).

MODIS-based analysis at the level of individual cities

A piecewise regression [30] was used to identify breakpoints of vegetation changes observed in MODIS NDVI time series for each city. We chose to focus on one breakpoint only in order to identify only the most substantial changes in urban vegetation over the past 20 years. A major breakpoint in the NDVI time series indicates that vegetation greenness has changed from browning to greening or vice versa (reversal). The vegetation greenness change is classified as Greening or Browning if no breakpoint is detected and the associated significant trend ($P \leq 0.05$) in NDVI during 2000 to 2020 is either positive or negative throughout the entire period. We use the class Stable if no breakpoint is detected and no significant ($P > 0.05$) NDVI trends are detected during 2000 to 2020. The class is named Reversal if vegetation dynamics change after breakpoints from greening to browning, and finally, Recovery implies that vegetation greenness greening after an initial browning.

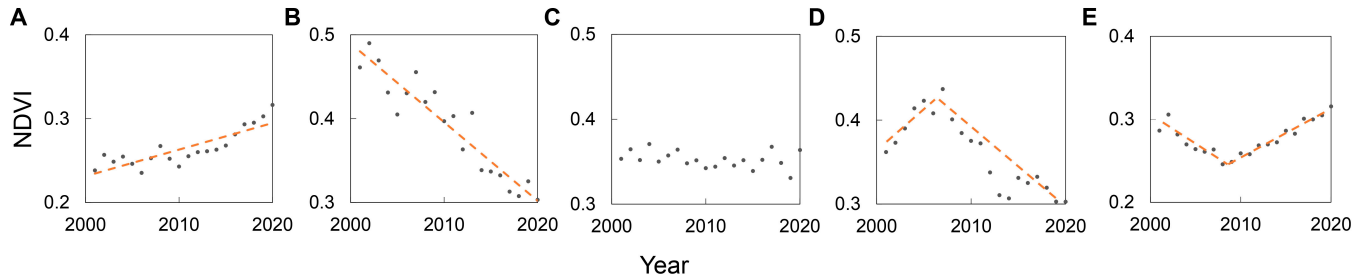

Fig. 2. Conceptual examples for urban change types using annual NDVI time series. (A) Greening. (B) Browning. (C) Stable. (d) Reversal. (E) Recovery.

Landsat-based analysis within urban areas

The Landsat-based Detection of Trends in Disturbance and Recovery algorithm (LandTrendr, https://emapr.github.io/LT-GEE/) implemented in the Google Earth Engine platform [31] was applied to detect vegetation dynamics and identify vegetation greenness change types within urban regions for each pixel. LandTrendr is a temporal segmentation method [23], which means that it identifies disturbances in time series of vegetation indices and classifies the periods between disturbances as temporal segments. It is used for dynamic mapping and monitoring of land vegetation disturbances and recovery at a spatial resolution of 30 m. The annual medoid NDVI values were used as inputs for LandTrendr [23]. We set the significance threshold for the model fitting used to smooth the time series to 0.05 and the maximum number of segments to 6 for the 20-year time period. Other parameters were unchanged [23]. The outputs are the number of segments and their duration, as well as the magnitude of the disturbances in NDVI units.

To find expressive thresholds defining the classes "increase" and "decrease" of a segment, we studied NDVI changes over 10 sites that have stable urban condition, such as airport, central train station, and historical buildings (Fig. S4). We found that NDVI fluctuations in these supposedly stable areas around −0.01 and 0.01, leading to a set of thresholds as follows: increase (magnitude ≥ 0.01), stable (−0.01 < magnitude < 0.01), and decrease (magnitude ≤ −0.01). Pixels that had more than 4 segments, suggesting multiple disturbances, were not included

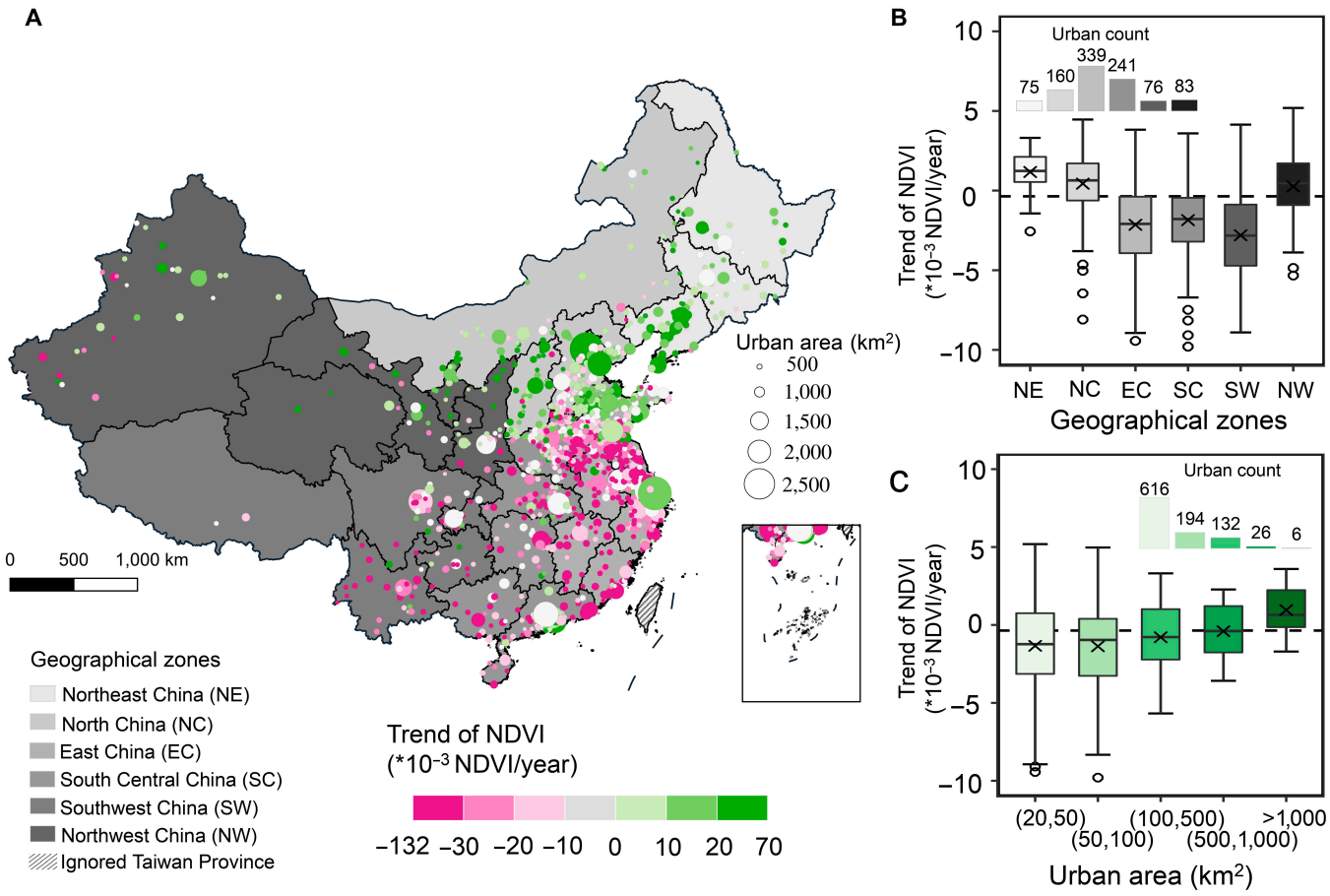

Fig. 3. NDVI change in urban areas in China during 2000 to 2020, including urban core and urbanization areas. (A) Mean NDVI trend at the level of individual cities during 2001 to 2020 (n = 965). (B) NDVI trends for urban areas stratified into different geographical zones. (C) NDVI trends for urban areas grouped by their size.

in this study (Fig. S5). We classified each pixel into 1 of the 5 vegetation change types (Greening, Browning, Stable, Reversal, and Recovery) based on the following rules: Pixels characterized by a disturbance in the form of an increase with stable conditions before/after were classified as Greening, whereas pixels showing a disturbance of the type decrease with otherwise stable segments are classified as Browning; pixels were classified as Stable if all segments were stable; pixels were classified as Reversal if the last segment showed a decrease or stable conditions following one or several segments with an increase; pixels were classified as Recovery if the last segment showed an increase or is stable following a segment with a decrease. More information is found in Table S1.

Results

Urban expansion and vegetation dynamics in China

The urban areas of the 974 studied cities covered an area of 72,785 km^2 in 2020, which is twice as much as compared to the cover in 2000 (36,400 km^2, Fig. S4). Urban expansion areas are primarily found in agglomeration areas (interconnected cities), such as Beijing–Tianjin, Yangtze River Delta, and the Pearl River Delta (Fig. S4). A total of 81.38% of the urban expansion areas were previously cropland, 10.11% were grassland, and 6.01% forest in 2000 (Fig. S6).

Urban greenness shows an overall positive trend during 2001 to 2020 for the majority of the cities in Northern China. These urban expansion areas had generally low greenness values in 2001 (Fig. S7), likely because the new built-up areas expanded into grasslands and croplands. Contrary, cities in Southern China usually expanded into former forests areas, resulting in negative greenness trends in urban areas (Fig. 3A and B). We subsequently classified cities by the size of their urban areas in 2020 and found that positive trends are observed mostly in large cities (> 500 km^2), whereas smaller cities (< 100 km^2) show a negative trend in greenness (Fig. 3A and C).

Overall, the NDVI trend for urban areas shows a slight browning during 2001 to 2020 (blue line in Fig. 4A). This negative trend is mostly found in the urban expansion areas (yellow line in Fig. 4A), whereas urban core areas show an increasing NDVI trend over this period. Looking closer at the time series, decreasing NDVI trends in urban areas were mostly found before 2010, and after 2011, a greening was found both in urban core and urban expansion areas, almost balancing the browning from urban expansion areas during the first period at national scale (Fig. 4A). These nonlinear NDVI dynamics for urban areas are studied in more details in the following sections.

Vegetation changes at city level

We used MODIS NDVI time series to study urban greenness changes at the level of individual cities (Fig. 4B). Out of the 974

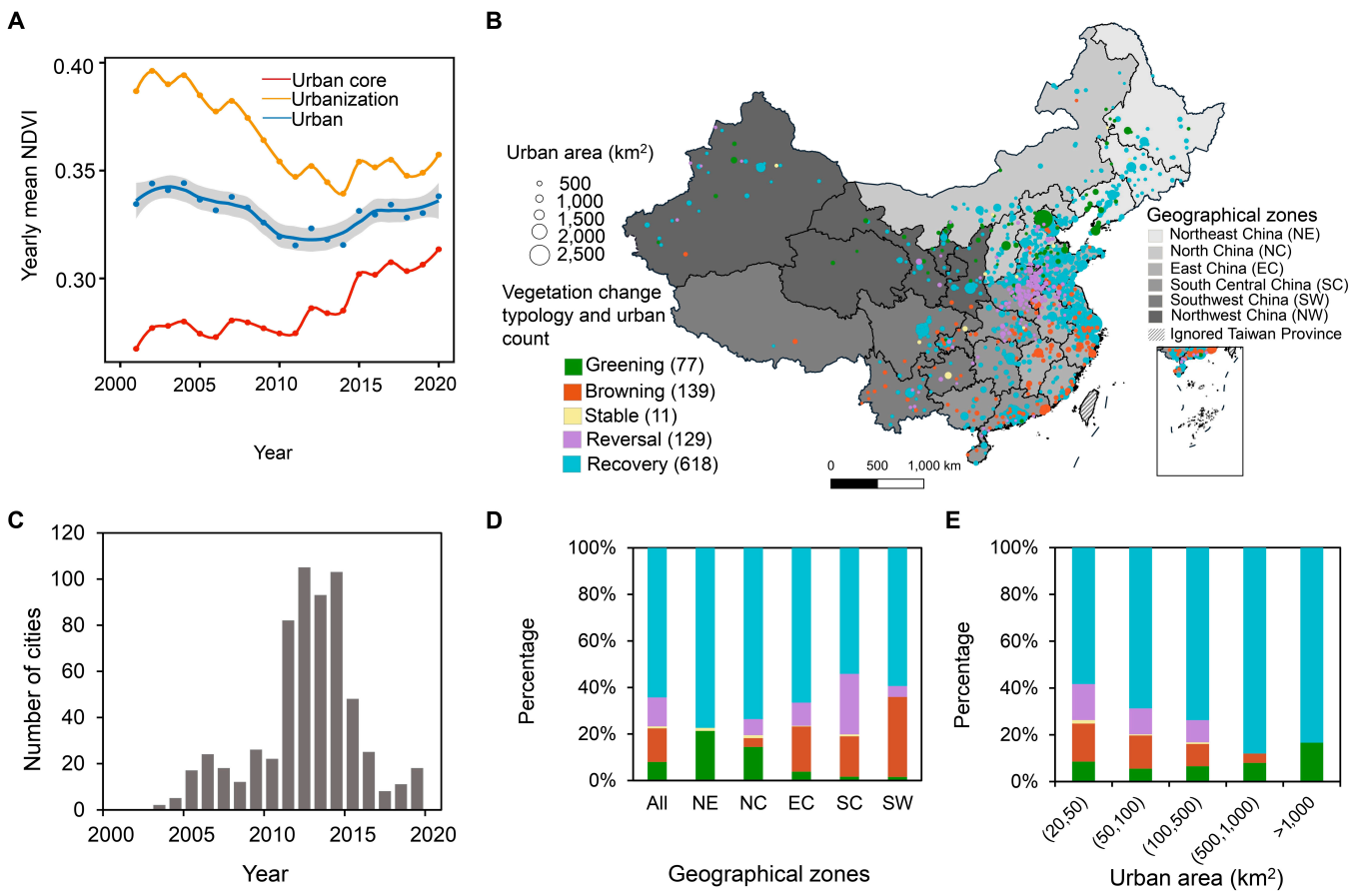

Fig. 4. Change types of MODIS NDVI in urban areas for 2001 to 2020. (A) Yearly mean NDVI in urban core and urban expansion areas during 2001 to 2020. (B) Vegetation change types for each urban areas (n = 965), including urban core and urbanization. (C) Number and timing of breakpoints of the class recovery (n = 609). (D) Percent of urban vegetation cover change types for different geographical zones. (E) Percent of vegetation change types for groups of different urban area sizes.

studied cities, 609 cities (63.45%) experienced a greening in NDVI after an initial browning. Breakpoints reflecting a change from browning to greening (recovery) were mainly found during 2011 to 2015 (Fig. 4C). These cities are distributed across all geographical zones in China regardless of the size of urban areas (Fig. 4B, D, and E). There are 77 cities (7.91% of all cities) that show a continuously greening NDVI trend, and most of these are large cities located in northern China (Fig. 5B and D). In total 139 cities (14.27%) show a continuously browning NDVI trend during 2000 to 2020, mainly located in Southern China (Fig. 4B and D). Nonsignificant trends (stable) are observed in 11 cities. For 129 cities (13.24%), mostly large cities in Central China, we found a reversal trend in urban greenness during 2000 to 2020, which reflects a change from greening to browning (Fig. 4B).

Vegetation changes within cities

We used Landsat time series to study urban greenness change types at higher spatial resolution for the 974 cities (visualization link: https://ee-xzrscph.projects.earthengine.app/view/change-type-of-urban-vegetation). We selected 2 cities (Shanghai in Fig. 5A, Chengdu in Fig. 5B) to showcase examples of the spatial patterns of the 5 change types within the city boundaries (Fig. 5). Distinct patterns of clustered change types are observed: greening and stable dominate urban cores, possibly due to the promotion of green spaces (e.g., urban parks) replacing residential and permanent built-up areas (Fig. 5C1 to C3). Built-up areas in both residential areas (Fig. 5D1 to D3) or former croplands (Fig. 5E1 to E3) are often classified as recovery, reflecting the initial loss of green vegetation during the transformation of croplands to artificial surface partly compensated by a following planting of trees in residential areas. The change types reversal and browning are mostly found in large industrial areas (Fig. 5E1 to E3 and F1 to F3).

We summed the pixel-level change types of all 974 cities and found that the class stable covers 25.26% of the urban areas, browning covers 24.55%, recovery 22.80%, greening 19.91%, and reversal 7.46% (Fig. 6A). In urban core areas the class stable (33.03%) and greening (25.44%) dominate, while browning (31.32%) and recovery (26.18%) are dominating in urban expansion areas (2000 to 2020) (Fig. 6A). We then selected 5 cities to illustrate different dominating patterns of change: greening both in urban core and urban expansion areas in Beijing (Fig. 6B), browning in urban expansion areas in Fuyang (Fig. 6C), stable in most areas in the smaller city of Togtoh (Fig. 6D), a reversal in the expansion areas of Luohe reflects recent vegetation losses (Fig. 6E) and recovery dominates expansion areas of Changzhou (Fig. 6F).

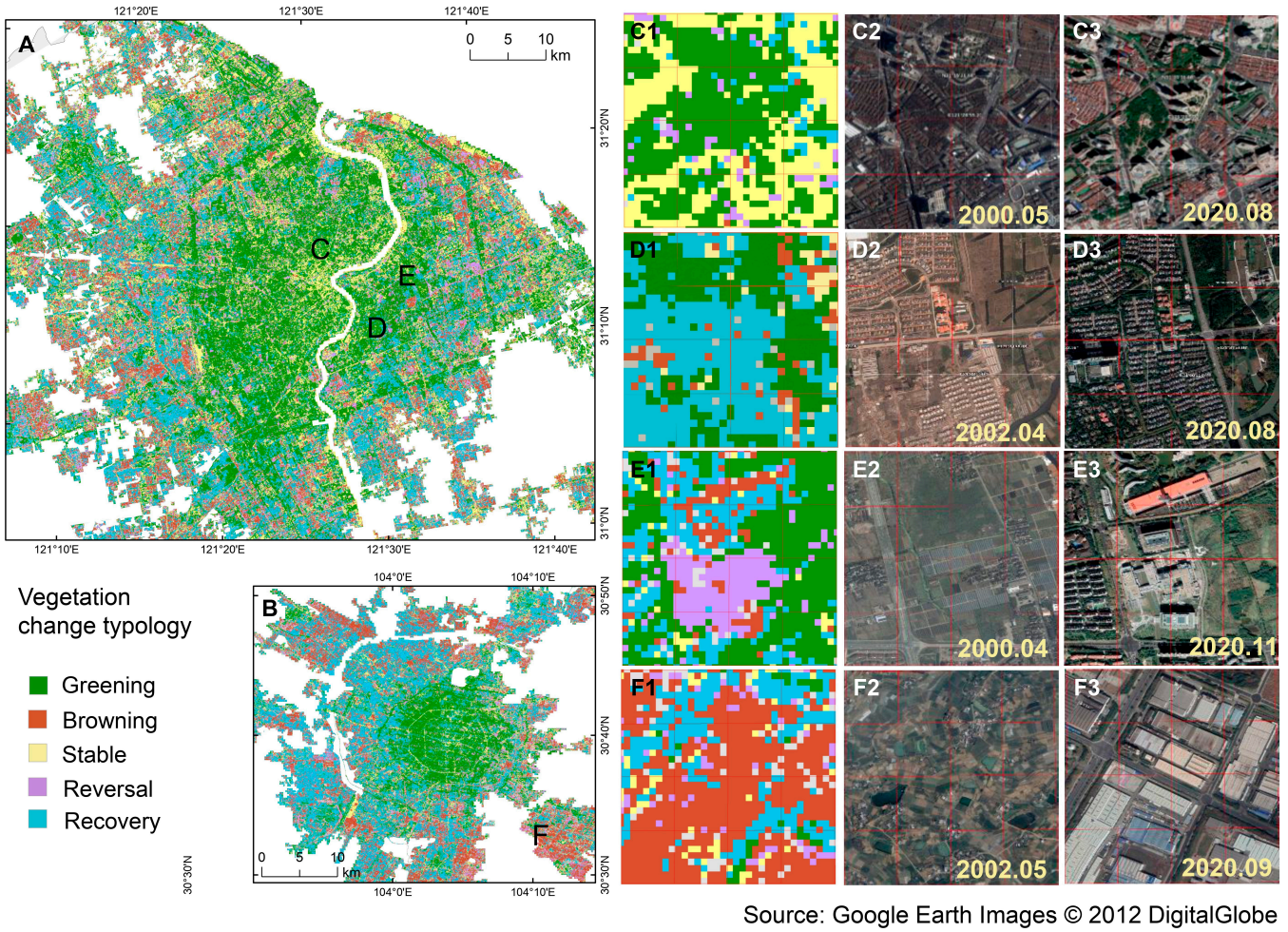

Fig. 5. Urban greenness changes (2000 to 2020) based on Landtrendr. (A) Shanghai. (B) Chengdu. (C1 to F1) Close ups showing examples. (C2 to F2) High-resolution images from Google Earth historical images from 2000 to 2002. (C3 to F3) Google Earth images for 2020.

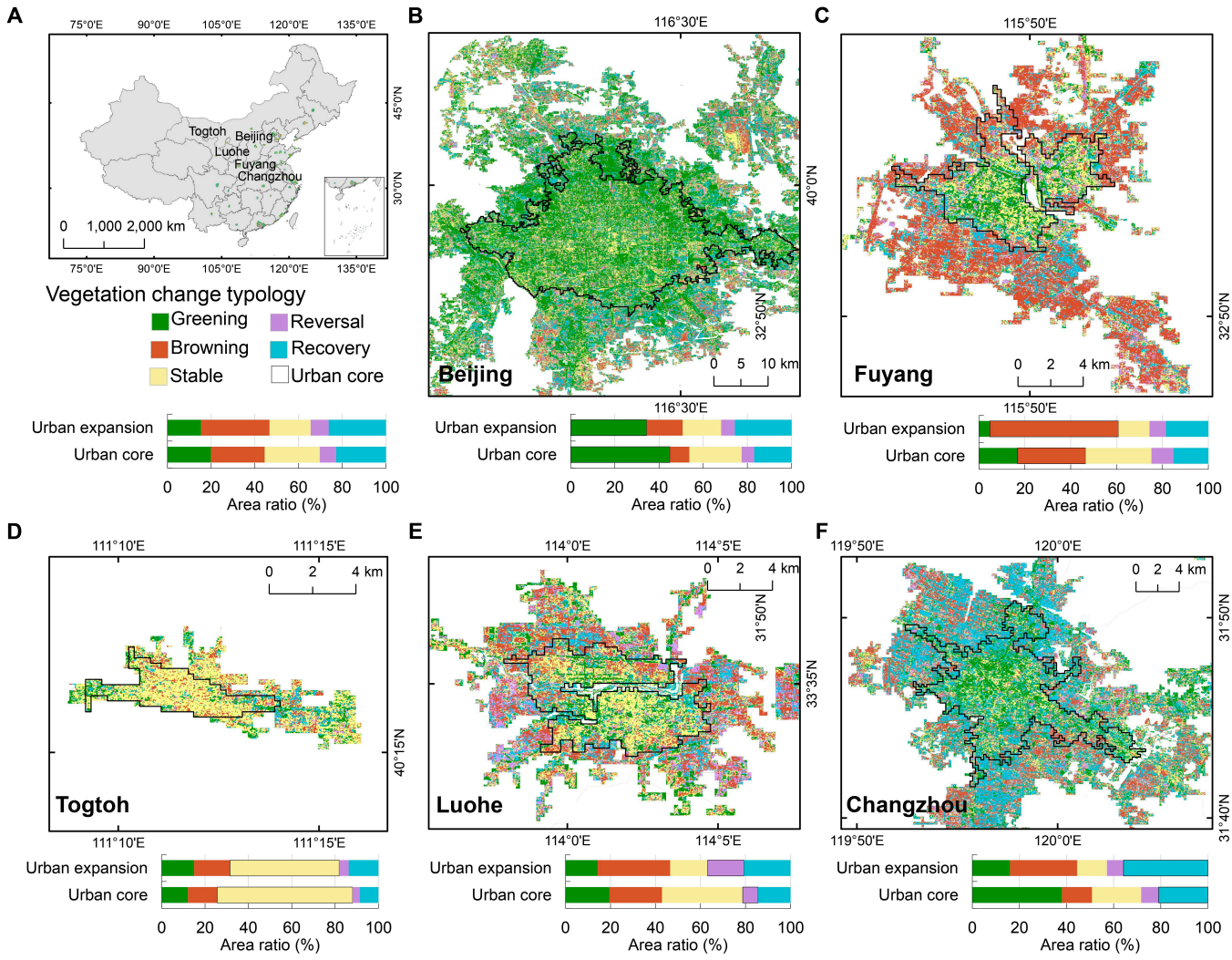

Fig. 6. Urban greenness changes for selected cities (2000 to 2020). (A) Vegetation change typology for entire cities in China (visualization link: https://ee-xzrscph.projects.earthengine.app/view/change-type-of-urban-vegetation). (B) Example city dominated by pixels classified as greening; (C) browning; (D) stable; (E) reversal; (F) recovery. The black line in the maps represent the urban core in 2000. The surrounding areas represent urban expansion areas. The dominating change type is highlighted by a black border in the bar plots.

Discussion

Urban expansion reduces natural vegetation cover, which threatens ecosystem services such as biodiversity and carbon stocks [3]. Browning in urban vegetation cover was observed in many developing countries while urban greening dominates cities of developed counties [32]. Urban greening projects and nature-based solutions are promoted in OECD (Organization for Economic Cooperation and Development) countries [33] to favor a greener living environment and to address adaptation to climate change. Examples are the URBAN GreenUP program initialized by the European Union [34], the "Greening the City" project in Australia [35], and the urban resilience program in Japan [36]. China has experienced an unprecedented urban expansion over the past decades globally, which has caused an initial loss of vegetation cover [37]. However, vegetation greenness was shown to increase again since 2011, nearly balancing the initial browning over the entire period 2000 to 2020. Explanations shown here are vegetation growth in urban core areas and more green spaces in newly built resident areas [38]. The timing of urban vegetation recovery corresponds to the start of the implementation of the national-scale urban greening policy [17]. National development strategies in China emphasized a rapid and large scale urban expansion before the 2011 but then paid more attention to promote urban sustainability and the quality of community [39]. In addition, urban expansion in China is mostly at the expense of agricultural land and only few forests are converted [2]. This explains the limited loss of vegetation but raises concerns about the loss of arable land and increased dependency on imported goods [40,41]. The urban greening may partly be contributed to by the enhancement of vegetation growth under a warmer urban climate with increasing CO_2 concentrations [42]. Yet, if the urban heat island and CO_2 fertilization effects should be dominating, we would expect the observed greening to be more continuous over time, but here, we show that the greening starts around 2010 and is mainly limited to the urban cores.

At a global scale, urban vegetation changes are mostly related to population growth and economic development with clear differences between continents [13]. Chinese cities show a rather

heterogeneous pattern on vegetation greenness changes, which may partially be explained by local land use policies at city level. For example, tree planting in Beijing causes increasing vegetation greenness both in urban core and urban expansion areas (e.g., One Million-Mu Plain afforestation Project) [43]. However, many smaller cities show an overall negative vegetation greenness trend, especially in southern China, where urban areas expanded into forests and natural shrublands (Fig. S3). Proper urban planning and management focusing on offsetting the vegetation loss caused by urban expansion requires accurate and timely information of urban vegetation change types in these emerging cities. The nonlinear vegetation change type mapping at both city and pixel levels as demonstrated in the present study is expected to be a useful tool in support of strategic planning.

Globally, urban greening is driven by vegetation greening in sparsely populated periurban areas [32]. However, we found that the recent greening of China's cities is driven by changes in urban core areas, supported by considerable increase in urban parks and a decline in industrial areas, whereas expansion areas are only most recently showing first signs of greening [14]. The establishment of new industrial zones drives ongoing vegetation loss in many periurban areas and is difficult to compensate [32]. In contrast, residential areas in the periurban areas mostly contribute to vegetation gains [32], and it is largely up to municipality governments to implement regulations to protect and increase vegetation cover in new urban areas.

Improved monitoring capacities from satellite images allow to assess urban vegetation cover at a high temporal and spatial resolution at national scale [13]. Rapid and timely city-level monitoring using coarse spatial resolution time series is essential to understand dominant characteristics of urban greenness at national scale; however, these results are of limited use from a management perspective. Therefore, detailed analyses from Landsat time series can be better linked to local land use/cover transformations [23,44], such as the establishment of street trees, small lawns, and residential parks [38]. These results are directly usable at the policy level and can feed into proactive management of ecosystem services of cities. Although the usage of time series segment methods to study vegetation cover trend and change of terrestrial ecosystems [23] have become a common tool available in cloud computing facilities like Google Earth Engine platform [31] such approaches has yet to be consolidated for use in analysis of urban ecosystems. Together with the pioneering studies [10,38,39], the present study supports the usage of segmentation approaches that unveil the multidirectional spatial-temporal urban vegetation change.

Conclusions and Perspectives

The rapid urbanization in China has caused international concerns on environmental pollution and the loss of natural vegetation. Here, we observe an abrupt change in urban greenness trends for the majority of the Chinese cities around 2010. This abrupt reversal from browning to greening follows political urban greening strategies implemented after 2010. Our major findings suggest that the greening of urban core areas nearly compensates for losses from urban expansion areas and also that even expansion areas show first signs of greening. It is remarkable to see how clearly policies are reflected in satellite time series, which serves as a powerful monitoring tool that can be applied to identify areas and cities that do not follow the general patterns. This study is based on analysis of a "greening/browning" variable, serving as an integral measure for vegetation cover and density. This variable does not provide any information on the composition of the vegetation, or quantitative measures on vegetation cover and biomass. Ecosystem services provided by urban greenness depend among others on the proportion between trees and grasses, and future studies need to go beyond greenness and quantify urban tree cover changes.

Acknowledgments

Funding: This work was supported by the China Scholarship Council (CSC, grant no. 201904910835 to X.Z.); Independent Research Fund Denmark–DFF Sapere Aude (grant 9064-00049B to M.B.); and the Villum Foundation through the project "Deep Learning and Remote Sensing for Unlocking Global Ecosystem Resource Dynamics" (DeReEco to R.F.).
Author contributions: X.Z. conceived and designed the study. X.Z. and Xiaoye T. drafted the first manuscript, and all authors contributed the discussion, review, and final version of the manuscript.
Competing interests: The authors declare that they have no competing interests.

Data Availability

MODIS NDVI time series including MOD13Q1 C6 (https://developers.google.com/earth-engine/datasets/catalog/MODIS_061_MOD13Q1) and MYD13Q1 C6 (https://developers.google.com/earth-engine/datasets/catalog/MODIS_061_MYD13Q1) can be accessed on Google Earth Engine. The GlobaLand30 land cover dataset is provided by https://www.webmap.cn/commres.do?method=globeIndex. Additionally, Suomi National Polar-orbiting Partnership (NPP) Satellite Visible Infrared Imaging Radiometer Suite (VIIRS) nighttime light data is available on Google Earth Engine by https://developers.google.com/earth-engine/datasets/catalog/NOAA_VIIRS_DNB_ANNUAL_V21.

Supplementary Materials

Figs. S1 to S7
Table S1

References

1. United Nations, Department of Economic and Social Affairs, Population Division. *World population prospects 2019: Highlights (ST/ESA/SER.A/423)*. New York (NY): United Nations; 2019.
2. Liu X, Huang Y, Xu X, Li X, Li X, Ciais P, Lin P, Gong K, Ziegler AD, Chen A, et al. High-spatiotemporal-resolution mapping of global urban change from 1985 to 2015. *Nat Sustain*. 2020;3:564–570.
3. Seto KC, Güneralp B, Hutyra LR. Global forecasts of urban expansion to 2030 and direct impacts on biodiversity and carbon pools. *Proc Natl Acad Sci*. 2012;109(40):16083–16088.
4. Sun L, Chen J, Li Q, Huang D. Dramatic uneven urbanization of large cities throughout the world in recent decades. *Nat Commun*. 2020;11(1):5366.
5. Fletcher DH, Likongwe PJ, Chiotha SS, Nduwayezu G, Mallick D, Md NU, Rahman A, Golovátina-Mora P, Lotero L, Bricker S, et al. Using demand mapping to assess the benefits

of urban green and blue space in cities from four continents. *Sci Total Environ*. 2021;785:147238.
6. Gozalo GR, Morillas JMB, González DM, Moraga PA. Relationships among satisfaction, noise perception, and use of urban green spaces. *Sci Total Environ*. 2018;624:438–450.
7. Yuan F, Bauer ME. Comparison of impervious surface area and normalized difference vegetation index as indicators of surface urban heat island effects in Landsat imagery. *Remote Sens Environ*. 2007;106(3):375–386.
8. Donovan GH, Gatziolis D, Longley I, Douwes J. Vegetation diversity protects against childhood asthma: Results from a large New Zealand birth cohort. *Nat Plants*. 2018;4(6): 358–364.
9. Engemann K, Pedersen CB, Arge L, Tsirogiannis C, Mortensen PB, Svenning J-C. Residential green space in childhood is associated with lower risk of psychiatric disorders from adolescence into adulthood. *Proc Natl Acad Sci USA*. 2019;116(11):5188–5193.
10. Pandey B, Zhang Q, Seto KC. Time series analysis of satellite data to characterize multiple land use transitions: A case study of urban growth and agricultural land loss in India. *J Land Use Sci*. 2018;13(3):221–237.
11. Liu Y, Wang Y, Peng J, Du Y, Liu X, Li S, Zhang D. Correlations between urbanization and vegetation degradation across the World's metropolises using DMSP/OLS nighttime light data. *Remote Sens*. 2015;7(2):2067–2088.
12. Yao R, Cao J, Wang L, Zhang W, Wu X. Urbanization effects on vegetation cover in major African cities during 2001-2017. *Int J Appl Earth Obs Geoinfor*. 2019;75:44–53.
13. Zhang W, Randall M, Jensen MB, Brandt M, Wang Q, Fensholt R. Socio-economic and climatic changes lead to contrasting global urban vegetation trends. *Glob Environ Change*. 2021;71:102385.
14. Fu Y, Li J, Weng Q, Zheng Q, Li L, Dai S, Guo B. Characterizing the spatial pattern of annual urban growth by using time series Landsat imagery. *Sci Total Environ*. 2019;666:274–284.
15. Zhang X, Brandt M, Tong X, Ciais P, Yue Y, Xiao X, Zhang W, Wang K, Fensholt R. A large but transient carbon sink from urbanization and rural depopulation in China. *Nat Sustain*. 2022;5:321–328.
16. Bryan BA, Gao L, Ye Y, Sun X, Connor JD, Crossman ND, Stafford-Smith M, Wu J, He C, Yu D, et al. China's response to a national land-system sustainability emergency. *Nature*. 2018;559:193–204.
17. Feng D, Bao W, Yang Y, Fu M. How do government policies promote greening? Evidence from China. *Land Use Policy*. 2021;104:105389.
18. Den Hartog H. Engineering an ecological civilization along Shanghai's main waterfront and coastline: Evaluating ongoing efforts to construct an urban eco-network. *Front Environ Sci*. 2021;9: 10.3389/fenvs.2021.639739.
19. Gare A. China and the struggle for ecological civilization. *Capital Nat Social*. 2012;23(4):10–26.
20. Li D, Wu S, Liang Z, Li S. The impacts of urbanization and climate change on urban vegetation dynamics in China. *Urban For Urban Green*. 2020;54:126764.
21. Nichol J, Lee CM. Urban vegetation monitoring in Hong Kong using high resolution multispectral images. *Int J Remote Sens*. 2005;26(5):903–918.
22. Wulder MA, Loveland TR, Roy DP, Crawford CJ, Masek JG, Woodcock CE, Allen RG, Anderson MC, Belward AS, Cohen WB, et al. Current status of Landsat program, science, and applications. *Remote Sens Environ*. 2019;225:127–147.
23. Kennedy RE, Yang Z, Cohen WB. Detecting trends in forest disturbance and recovery using yearly Landsat time series: 1. LandTrendr—Temporal segmentation algorithms. *Remote Sens Environ*. 2010;114(12):2897–2910.
24. Chen F, Chen J, Wu H, Hou D, Zhang W, Zhang J, Zhou X, Chen L. A landscape shape index-based sampling approach for land cover accuracy assessment. *Sci China Earth Sci*. 2016;59:2263–2274.
25. Chen J, Chen J, Liao A, Cao X, Chen L, Chen X, He C, Han G, Peng S, Lu M, et al. Global land cover mapping at 30 m resolution: A POK-based operational approach. *ISPRS J Photogramm Remote Sens*. 2015;103:7–27.
26. Levin N, Kyba CCM, Zhang Q, Sánchez de Miguel A, Román MO, Li X, Portnov BA, Molthan AL, Jechow A, Miller SD, et al. Remote sensing of night lights: A review and an outlook for the future. *Remote Sens Environ*. 2020;237:111443.
27. Elvidge CD, Zhizhin M, Ghosh T, Hsu F-C, Taneja J. Annual time series of global VIIRS nighttime lights derived from monthly averages: 2012 to 2019. *Remote Sens*. 2021;13:922.
28. Small C, Pozzi F, Elvidge CD. Spatial analysis of global urban extent from DMSP-OLS night lights. *Remote Sens Environ*. 2005;96(3-4):277–291.
29. Zhang X, Guo S, Guan Y, Cai D, Zhang C, Fraedrich K, Xiao H, Tian Z. Urbanization and spillover effect for three megaregions in China: Evidence from DMSP/OLS nighttime lights. *Remote Sens*. 2018;10(12):1888.
30. Muggeo VMR. Estimating regression models with unknown break-points. *Stat Med*. 2003;22(19):3055–3071.
31. Kennedy RE, Yang Z, Gorelick N, Braaten J, Cavalcante L, Cohen WB, Healey S. Implementation of the LandTrendr algorithm on google earth engine. *Remote Sens*. 2018;10(5):691.
32. Richards DR, Belcher RN. Global changes in urban vegetation cover. *Remote Sens*. 2020;12(1):23.
33. Lindholst AC. Contracting-out in urban green-space management: Instruments, approaches and arrangements. *Urban For Urban Green*. 2009;8(4):257–268.
34. O'Sullivan F, Mell I, Clement S. Novel solutions or rebranded approaches: Evaluating the use of nature-based solutions (NBS) in Europe. *Front Sustain Cities*. 2020;2:572527.
35. Fastenrath S, Bush J, Coenen L. Scaling-up nature-based solutions. Lessons from the Living Melbourne strategy. *Geoforum*. 2020;116:63–72.
36. Augusto B, Roebeling P, Rafael S, Ferreira J, Ascenso A, Bodilis C. Short and medium-to long-term impacts of nature-based solutions on urban heat. 2020;57:102122.
37. Liu X, Pei F, Wen Y, Li X, Wang S, Wu C, Cai Y, Wu J, Chen J, Feng K, et al. Global urban expansion offsets climate-driven increases in terrestrial net primary productivity. *Nat Commun*. 2019;10:5558.
38. Shahtahmassebi AR, Li C, Fan Y, Wu Y, Lin Y, Gan M, Wang K, Malik A, Blackburn GA. Remote sensing of urban green spaces: A review. *Urban For Urban Green*. 2021;57:126946.
39. Deng C, Liu J, Nie X, Li Z, Liu Y, Xiao H, Hu X, Wang L, Zhang Y, Zhang G, et al. How trade-offs between ecological construction and urbanization expansion affect ecosystem services. *Ecol Indic*. 2021;122:107253.

40. Deng X, Huang J, Rozelle S, Zhang J, Li Z. Impact of urbanization on cultivated land changes in China. *Land Use Policy*. 2015;45:1–7.
41. van Vliet J. Direct and indirect loss of natural area from urban expansion. *Nat Sustain*. 2019;2:755–763.
42. Zhao S, Liu S, Zhou D. Prevalent vegetation growth enhancement in urban environment. *Proc Natl Acad Sci*. 2016;113(22):6313–6318.
43. Yao N, van den Bosch CCK, Yang J, Devisscher T, Wirtz Z, Jia L, Duan J, Ma L. Beijing's 50 million new urban trees: Strategic governance for large-scale urban afforestation. *Urban For Urban Green*. 2019;44:126392.
44. Cohen WB, Yang Z, Healey SP, Kennedy RE, Gorelick N. A LandTrendr multispectral ensemble for forest disturbance detection. *Remote Sens Environ*. 2018;205:131–140.